1 # Assessing contributions of natural surface and anthropogenic emissions to

2 # atmospheric mercury in a fast developing region of Eastern China from

3 # 2015 to 2018

4 Xiaofei Qin[1], Leiming Zhang[2], Guochen Wang[1], Xiaohao Wang[3], Qingyan Fu[3,4], Jian Xu[1], Hao Li[1],

5 Jia Chen[1], Qianbiao Zhao[3,4], Yanfen Lin[3,4], Juntao Huo[3,4], Fengwen Wang[5], Kan Huang[1,6,7*],

6 Congrui Deng[1,*]

8 [1] Center for Atmospheric Chemistry Study, Shanghai Key Laboratory of Atmospheric Particle
9 Pollution and Prevention (LAP3), Department of Environmental Science and Engineering, Fudan
10 University, Shanghai, 200433, China
11 [2] Air Quality Research Division, Science and Technology Branch, Environment and Climate Change
12 Canada, Toronto, M3H 5T4, Canada
13 [3] Shanghai Environmental Monitoring Center, Shanghai, 200030, China
14 [4] State Ecologic Environmental Scientific Observation and Research Station for Dianshan Lake,
15 Shanghai 201713, China
16 [5] State Key Laboratory of Coal Mine Disaster Dynamics and Control, College of Environment and
17 Ecology, Chongqing University, Chongqing 400030, China
18 [6] Institute of Eco-Chongming (IEC), Shanghai, 202162, China
19 [7] Institute of Atmospheric Sciences, Fudan University, Shanghai 200433, China

21 **Abstract**

22 Mercury (Hg) is a global toxic pollutant that can be released into the atmosphere through

23 anthropogenic and natural sources. The uncertainties in the estimated emission amounts are much

24 larger from natural than anthropogenic sources. A method was developed in the present study to

25 quantify the contributions of natural surface mercury emissions to ambient gaseous elemental

26 mercury (GEM) concentrations through application of positive matrix factorization (PMF) analysis

27 with temperature and NH_3 as indicators of GEM emissions from natural surfaces. GEM

28 concentrations were continuously monitored at a 2-hourly resolution at a regional background site

29 in the Yangtze River Delta in Eastern China during 2015-2018. Annual average GEM concentrations

30 were in the range of 2.03-3.01 ng/m³, with a strong decreasing trend at a rate of -0.32±0.07 ng m^{-3}

31 yr^{-1} from 2015 to 2018, which was mostly caused by reduced anthropogenic emissions since 2013.

32 The estimated contributions from natural surface emissions of mercury to the ambient GEM

33 concentrations were in the range of 1.00-1.13 ng/m³ on annual average with insignificant interannual

34 changes, but the relative contribution increased significantly from 41% in 2015 to 57% in 2018,

35 gradually surpassing those from anthropogenic sources.

36

1. Introduction

Mercury has long been recognized as a toxic pollutant due to its bioaccumulation and health effects (Driscoll et al., 2013b;Clarkson and Magos, 2006;Schroeder and Munthe, 1998;Horowitz et al., 2017;Fu et al., 2012;Wright et al., 2018). Mercury in the atmosphere can be transported globally, mostly in the form of gaseous elemental mercury (GEM) due to its long lifetime in air (Driscoll et al., 2013a). Clarifying sources and quantifying emissions from the major sources of atmospheric mercury are critical for understanding the biogeochemical cycle of mercury and developing mercury reduction strategies. Mercury in the atmosphere is released from both natural and anthropogenic sources. Natural sources include volcanoes. geological weathering, forest fires, re-emissions of pre-deposited mercury from natural surfaces, etc (Gustin et al., 2008;Mason and Sheu, 2002). Among these sources, emissions from natural surfaces are the major ones and a number of studies have been devoted to understanding the processes of natural surface emissions (Xu et al., 1999;Lindberg et al., 2002;Kocman et al., 2013). Anthropogenic sources mainly include coal-fired power plants, non-ferrous metal smelters, and waste incineration (Friedli et al., 2009). Globally, natural sources released about 5200 tons mercury into the atmosphere on an annual basis, which contributed up to two-thirds of the global atmospheric mercury budget, while those by anthropogenic sources was estimated to be around 2300 tons (Pirrone et al., 2010). In China, the total mercury emissions released from natural and anthropogenic sources were estimated to be 574.5 ton yr^{-1}, and 571 ton yr^{-1}, respectively (Wang et al., 2016;Zhang et al., 2015).

During the past decades, anthropogenic emissions of mercury in Europe and North America have been reduced significantly through phasing out mercury from many commercial products as well as benefiting from SO_2 and NO_x emission reduction from coal-fired utilities, resulting in considerable decrease in atmospheric mercury concentrations in these regions (e.g., approximately 1-2% yr^{-1} decrease from 1990 to 2013) (Streets et al., 2011;Zhang et al., 2016). In China, anthropogenic mercury emissions decreased from 571 ton in 2013 to 444 ton in 2017 due to the co-benefits of aggressive air pollutant control measures implemented in this period (Liu et al., 2019a). GEM concentrations measured at a rural site north of Shanghai showed a substantially decreasing trend from 2014 to 2016 (Tang et al., 2018).

With the decrease of anthropogenic mercury emissions in many parts of the world (Zhang et al., 2016), the contributions of natural emissions to total mercury budget are expected to be more

67 important. However, the trends of natural emissions are still unclear due to the difficulties in directly

68 measuring GEM emissions from natural surfaces (Zhu et al., 2015). Existing estimates of GEM

69 emission from natural sources have large uncertainties (e.g., from 1500 to 5207 Mg yr^{-1} on global

70 scale), limiting our understanding of the role of natural emissions in the global mercury cycle (Song

71 et al., 2015;Wang et al., 2014b). For example, a study at rural Beijing showed that modeled GEM

72 concentrations were underestimated by about 40% than measurements from April to September

73 2009 due to the absence of natural emission inventories (Wang et al., 2014a). Hence, it is meaningful

74 to develop a method to quantify the contributions of natural surface emissions to total mercury

75 budget in the atmosphere, especially in China where anthropogenic emissions have been fast

76 decreasing in recent years.

77   The purpose of the present study is to differentiate the contributions of natural surface

78 emissions and anthropogenic emissions to the measured ambient GEM concentrations collected

79 during a four-year period at a regional background site in the Yangtze River Delta (YRD) of Eastern

80 China. This was done by conducting positive matrix factorization (PMF) analysis with identified

81 variables as tracers of natural surface mercury emissions. Results presented in this study provide an

82 approach that can be potentially used for improving mercury emission databases for natural sources.

83

84 **2. Materials and methods**

85 **2.1 Site description**

86   Shanghai, situated in the YRD region, is one of the most developed cities in China. Like in

87 many other cities in China, severe air pollutions have occurred frequently in this city in the past

88 decades. A supersite has been set up next to the Dianshan Lake in Qingpu District of rural Shanghai

89 (Figure 1) as part of the framework of State Environmental Protection Scientific Observation and

90 Research Station. This supersite is designed to represent the regional scale air pollution

91 characteristics in the YRD region based on the following two considerations: (1) it is located in the

92 conjunction area of Shanghai, Jiangsu, and Zhejiang provinces; and (2) there are no large point

93 sources such as coal-fired power plants, nonferrous metal smelting, and cement production within

94 20km distance surrounding the site. This site was established in 2013 and its capacity has been

95 gradually built by measuring a set of atmospheric parameters, including meteorological factors,

96 trace gases, aerosol physical and chemical parameters, vertical profiles of ozone and particles, etc.

97   More detailed descriptions of the site can be found elsewhere (Qin et al., 2019;Duan et al., 2017).

98

99   **2.2 Measurements of gaseous elemental mercury**

100   An automated mercury vapor analyzer Tekran 2537B/1130/1135 was installed on the third floor

101   of a building for real time continuous GEM measurements since January 2015. GEM was measured

102   based on the principle of cold vapor atomic fluorescence spectroscopy (CVAFS) (Landis and Keeler,

103   2002). Briefly, ambient GEM was collected on gold traps and then thermally decomposed to GEM

104   before detection. The sampling interval of GEM was 5 minutes with a flow rate of 1L/min. More

105   details of this instrument can be found elsewhere (Mao et al., 2008).

106   Strict quality control procedures were followed during the sampling process. Denuders and

107   quartz filters were prepared and cleaned according to the instructions in Tekran technical notes

108   before sampling. Routine calibration with internal permeation source was performed every 47 hours

109   and manual injections of standard saturated mercury vapor were conducted to ensure the accuracy

110   of these automated calibrations. The KCl-coated denuder, Teflon-coated glass inlet, and impactor

111   plate were replaced weekly and quartz filters were replaced monthly. Individual extremely high

112   GEM concentrations that occasionally happened were regarded as outliers and were excluded from

113   the data analysis. In this study, the number of valid GEM data was 16266.

114

115   **2.3 Measurements of other air pollutants and meteorological parameters**

116   Water soluble ions in $PM_{2.5}$ and soluble gases were continuously measured by Monitor for

117   Aerosols and Gases in ambient Air (MARGA) operated at a flow rate of 16.7 L/min with a time

118   resolution of one hour, as detailed in (Chang et al., 2016). Briefly, water-soluble gases in the airflow

119   were removed by an absorbing liquid, then the particles were induced by a supersaturation of water

120   vapor to grow into droplets before they were collected and transported into the analytical chamber.

121   Trace metals in $PM_{2.5}$ were continuously measured by using the Xact 625 ambient metals

122   monitor (Cooper Environmental, Beaverton, OR, USA) operated at a flow rate of 16.7 L/min with

123   hourly resolution, as detailed in (Yu et al., 2019). Briefly, the particles in the airflow were deposited

124   onto a Teflon filter tape, and then transported into the spectrometer where the particles were

125   analyzed with an X-ray fluorescence. Black carbon in $PM_{2.5}$ was measured by a multiwavelength

126   Aethalometer (AE-33, Magee Scientific). Ambient particles were collected on a paper tape at a flow

127 rate of 5 L/min. Aerosol light absorptions of BC were measured at seven wavelengths of 370, 470,

128 520, 590, 660, 880, and 950nm.

129   Sulfur dioxide, carbon monoxide, and $PM_{2.5}$ were measured by Thermo Fisher 43i, Thermo

130 Fisher 48i-TLE, and Thermo Fisher 1405-F, respectively. Meteorological parameters including

131 ambient temperature, wind speed, and wind direction were obtained at the sampling site by using

132 the automatic weather station (AWS). Bivariate polar plots (BPP) were applied in this study to

133 explore how GEM concentrations change with different wind direction and wind speed, which has

134 proven to be a reliable method for identifying different source regions (Carslaw et al., 2006;Carslaw

135 and Ropkins, 2012;Chang et al., 2017). Here, the open-source software "openair" in R was used to

136 create BPPs (Carslaw and Ropkins, 2012).

137

138 **2.4 Positive matrix factorization (PMF)**

139   The PMF model has been proven to be a useful tool to provide quantitative source profiles and

140 source contributions (Xu et al., 2017;Gibson et al., 2015). The basic principle of PMF is that

141 concentrations of the samples were determined by the source profiles with different contributions,

142 which can be descried as follows:

143 $$X_{ij} = \sum_{k=1}^{P} g_{ik} f_{kj} + e_{ij} \quad (1)$$

144 where X_{ij} represents the concentration of the jth species in the ith sample, g_{ik} is the contribution

145 of the kth factor in the ith sample, f_{kj} provides the information of the mass fraction of the jth

146 species in the kth factor, e_{ij} is the residual for specific measurement, and P represents the number

147 of factors.

148   The objective function expressed in Eq. (2) below, which is the sum of the square of the

149 difference between the measured and modeled concentrations weighted by the concentration

150 uncertainties, needs to be minimized before the PMF model determines the optimal non-negative

151 factor profiles and contributions.(Cheng et al., 2015)

152 $$Q = \sum_{i=1}^{n} \sum_{j=1}^{m} \left(\frac{X_{ij} - \sum_{k=1}^{p} A_{ik} F_{kj}}{S_{ij}} \right)^2 (2)$$

153 where X_{ij} represents the concentration of the jth contamination in the ith sample, m is the total

154 number of pollutant, and n is the total number of sample. A_{ik} represents the contribution of the kth

155 factor on the ith sample and F_{kj} represents the mass fraction of the jth pollutant in the kth factor.

156 S_{ij} is the uncertainty of the jth pollutant on the ith factor and P is the number of factors. In this

157   study, we explored the number of factors from three to eight with the optimal solutions determined

158   by the slope of the Q value versus the number of factors. For each run, the stability and reliability

159   of the outputs were assessed by referring to the Q value, residual analysis, and correlation

160   coefficients between observed and predicted concentrations. Finally, we found that a six-factor

161   solution showed the most stable results and gave the most reasonable interpretation. A dataset

162   containing uncertainty values of each species was created and digested into the model, with the error

163   fraction being assumed to be 15% for GEM concentration and 10% for other compounds (Xu et al.,

164   2017;Polissar et al., 1998).

165   It should be noted that Fpeak model run at the strength of 0.5 was done by using the rotation

166   tools in PMF and the results were summarized in Table S1. For all seasons, the increase of the Q-

167   value due to the Fpeak rotation with a dQ was less than 1% of the Base Run Q (robust) value.

168   According to the User Guide of PMF5.0, it was acceptable when the %dQ was less than 5%. The

169   profiles and contributions of each source were examined and there were no significant differences

170   between the factor contributions of Base Run and rotation results. Hence, the Base Run results were

171   used in this study.

172

173   **2.5 Annual changes of anthropogenic mercury emission in China and YRD**

174   It was reported that the annual anthropogenic atmospheric mercury emission in China

175   significantly increased from 147 tons in 1978 to 549 tons in 2010 (Wu et al., 2016). In more recent

176   years, in order to cope with the severe air pollution situation, the Chinese government has taken

177   many rigorous and ambitious measures such as introduction of ultra-low emissions standards on

178   power plants and phasing out of small factories with high-emissions (Zheng et al., 2018). As a result,

179   mercury emissions from anthropogenic sources have since been declining in China. For the five-

180   year period of 2013-2017, annual total anthropogenic mercury emissions in China were estimated

181   to be 571, 547, 528, 486, and 444 tons, respectively, or a total decline of 127 tons. During the same

182   period, the reduction of anthropogenic mercury emissions reached 60 tons in eastern China (Liu et

183   al., 2019a).

184

185   **3. Results and Discussion**

186   **3.1 The measured gaseous elemental mercury**

3.1.1 Decreasing trend of gaseous elemental mercury

The measured annual mean GEM concentrations were 3.01 ± 1.03, 2.58 ± 0.84, 2.52 ± 0.84, and 2.03 ± 0.69 ng/m^3 from 2015 to 2018. By using the Theil-Sen function, monthly GEM exhibited a significantly decreasing trend from 2015 to 2018 ($p<0.05$) with a rate of -0.32 ± 0.07 ng m^{-3} yr^{-1} (Figure 2a). This decreasing trend was consistent with the trends of mass concentrations of PM$_{2.5}$ and SO$_2$ (Figure 2b & 2c), which were attributed to the implementation of the Clean Air Action since 2013 in China (Zheng et al., 2018). As mentioned earlier (Section 2.5), the nationwide reduction of anthropogenic mercury emissions should be largely responsible for the significant decrease in GEM concentration observed at the YRD regional background site.

Seasonal average GEM concentrations decreased from 3.62 ng/m^3 to 2.17 ng/m^3 with a rate of -0.37 ng m^{-3} yr^{-1} in spring, from 2.89 ng/m^3 to 1.98 ng/m^3 with a rate of -0.26 ng m^{-3} yr^{-1} in summer, from 2.62 ng/m^3 to 1.94 ng/m^3 with a rate of -0.22 ng m^{-3} yr^{-1} in autumn, and from 2.91 ng/m^3 to 1.82 ng/m^3 with a rate of -0.35 ng m^{-3} yr^{-1} in winter (Figure 3). The decreasing rates of GEM were $\sim30\%$ lower in the warm seasons than the cold seasons. Considering that seasonal variations of anthropogenic emission were less temperature dependent, the different seasonal decreasing rates of GEM between the warm and cold seasons should be mostly caused by the seasonal-dependent emission amounts from natural sources, knowing that natural surface emissions are controlled by solar radiation and temperature, among other factors (Howard and Edwards, 2018;Pannu et al., 2014;Mason, 2009).

3.1.2 Impact of temperature on ambient gaseous elemental mercury

In a previous study we showed that GEM concentrations tended to rise with increasing temperature in the YRD region, which was considered to be the effect of temperature-dependent emission amounts from natural surfaces (Qin et al., 2019). Here, to qualitatively investigate the role of natural surface emissions on ambient GEM concentration, diurnal profiles of the bi-hourly GEM concentration and temperature are exhibited in Figure 4. If looking at the whole year data together, moderate to high correlations were seen between the diurnal variations of GEM and temperature in 2016, 2017, and 2018 with R^2 being 0.30 to 0.86 ($p<0.05$), except in 2015 with little correlation with R^2 being only 0.03 ($p>0.05$) (Figure 4a-4d). The maximum GEM concentrations generally appeared around 10AM - 14PM, mostly coincided with daily peak temperature. These findings

217   provided strong evidence of temperature-dependent GEM sources.

218   Due to the large differences in ambient temperature between warm (from June to November)

219 and cold (from December to May) seasons in the YRD region, the effects of temperature-dependent

220 GEM sources on the ambient GEM concentrations should be different in different seasons. As

221 expected, high correlations between GEM concentrations and temperature were found in the warm

222 seasons with R^2 being in the range of 0.15 to 0.87 (Figures 4e-4h), while nearly no correlations in

223 the cold seasons (Figures 4i-4l). Thus, the influence of natural surface emissions on ambient GEM

224 concentration was important in the warm seasons, but may not be the case in the cold seasons. The

225 seasonal bivariate polar plots of GEM showed that high GEM concentrations were associated

226 frequently with air flows from the south and southwest and occasionally with those from the north,

227 particularly in summer (Figure S1). This was consistent with the findings in previous studies which

228 showed stronger natural surface emissions in South and Southwest China than North China (Wang

229 et al., 2016;Feng et al., 2005;Wang et al., 2006;Sommar et al., 2016). Hence, in the context of

230 significant reduction of anthropogenic mercury emission in China, especially in North China (Liu

231 et al., 2019b), natural surface emissions significantly impacted the ambient GEM concentrations at

232 this sampling site.

233

234 **3.2 Quantify the contributions from natural surface emissions to ambient gaseous elemental**

235 **mercury**

236 **3.2.1 Development of the approach**

237   A method is developed below for quantifying the contributions of GEM emissions from natural

238 surfaces to ambient GEM concentrations through application of the PMF model by introducing

239 specific variables related to natural surface emissions as traces. The first step is to identify what

240 variables are directly or indirectly related to the natural surface emissions of GEM. Temperature is

241 certainly a dominant one as has been demonstrated in existing soil-air fluxes studies of mercury

242 (Wang et al., 2014b;Zhu et al., 2016;Poissant and Casimir, 1998). The formation pathways of Hg^0

243 in soil are all related to temperature, an empirical rule suggests that a 10°C temperature increase

244 doubles the rates for chemical reaction near room temperature, which has been proven to be

245 applicable to Hg^{II} reduction in boreal soil (Moore and Carpi, 2005;Quinones and Anthony,

246 2011;Wang et al., 2016;Pannu et al., 2014). Discussions in Section 3.1.2 also suggested temperature

247   as a potentially useful tracer for predicting natural surface emissions of GEM. A second candidate

248   of tracers could be ambient NH_3 concentration because soil emissions of GEM and NH_3, both of

249   which are temperature-dependent, are treated in a similar way in air-quality modeling studies

250   (Wright and Zhang, 2015;Zhang et al., 2010). As shown in Figure S2, the mean diurnal variations

251   of GEM concentrations highly correlated with ambient temperature as well as NH_3. From this

252   perspective, NH_3 can be regarded as an indirect proxy for the natural surface emissions of GEM. In

253   a previous study, we have applied principal component analysis for source apportionment of

254   mercury in this area, and the source factor with high loadings for temperature and NH_3 was

255   interpreted as natural surface emissions of GEM (Qin et al., 2019).

256   Hence, in this study, we included the data of temperature and NH_3 into the PMF model to

257   apportion the sources of GEM. As shown in Figures S3-S18, the source apportionment results for

258   all the seasons of 2015-2018 all resolved a similar factor with high loadings of temperature and

259   moderate loadings of NH_3 and GEM. This factor was thought to be the natural surface emission

260   sources of mercury. As for the other resolved factors, the factor with high loadings of V and Ni

261   evidently represented shipping emissions, because Ni and V have been considered as typical tracers

262   of heavy oil combustion which has been commonly used in marine vessels (Viana et al., 2009). The

263   factor with high loading of Ca was assigned to cement production as the raw materials used in

264   cement production contain a large amount of calcium compounds. Moderate loadings of multiple

265   species including Cr, Mn, and Fe were found in one factor which was identified as iron and steel

266   production. The factor with high loading of NO was identified as vehicle emissions, as the major

267   source of NOx in the YRD region is mobile oil combustion (Tang et al., 2018). And the last factor

268   was identified as coal combustion due to the high loadings of As and Se, and moderate contributions

269   from Pb and SO_4^{2-}. As, Se, and Pb were all typical tracers of coal combustion and the precursor of

270   SO_4^{2-} (i.e. SO_2) also mainly derived from coal combustion.

271   In order to verify the PMF modeling results, we first examined the PMF model performance.

272   Table S2 shows the coefficient of determination (R^2) for GEM according to the observation-

273   prediction scatter plots (Figure S20-S23). The R^2 values ranged from 0.37 to 0.89, suggesting an

274   acceptable model performance. Figure S24-S27 display the time series of observed and predicted

275   GEM concentrations from 2015-2018, which revealed that, except for a few extremely high

276   observation values, the model can relatively well reproduce the observed GEM concentration on an

277   hourly basis.

278   To further verify the reliability of the resolved factors, the correlations between the mass

279   contributions of all factors to GEM and temperature were examined on the basis of diurnal profiles.

280   As shown in Figure S19, positive correlation was only found between the natural surface emissions

281   factor and temperature while the other resolved factors (i.e. vehicle emission, coal combustion,

282   shipping activities, cement production, and iron and steel production) did not show this relationship.

283   In addition, the relationship between particulate black carbon (BC) and GEM concentration was

284   investigated. On the one hand, BC mainly derived from various combustion processes, which were

285   also the main anthropogenic sources of atmospheric mercury. On the other hand, BC was never

286   introduced into the PMF modeling. As shown in Figure 5, the observed total GEM and BC

287   concentrations only showed weak correlations. This was mainly due to the fact that besides

288   anthropogenic sources, natural sources also contributed significantly to GEM. As a comparison,

289   anthropogenic GEM concentrations (extracted from PMF results) showed much better correlations

290   with BC from 2015 to 2018. In addition, the time-series of anthropogenic GEM concentrations

291   generally varied consistently with CO, which was also a tracer of fuel combustion (Figure S28). All

292   the evidences above corroborated that by using temperature and NH_3 as tracers for PMF modeling,

293   the separation of anthropogenic and natural GEM can be successfully achieved.

294   As for the specific anthropogenic mercury sources extracted from PMF results, Figure S29

295   shows that the time-series of coal combustion GEM also varied consistently with SO_2, indicating

296   that the coal combustion factor resolved by PMF was credible. As shown in Figure S30, the potential

297   source regions of shipping GEM were found mainly over coastal and oceanic areas, indicating the

298   shipping factor resolved in this study was also valid. Figure S31 and Figure S32 show that the PSCF

299   signals of cement production GEM were relatively weak in the YRD region, while there were

300   substantial high PSCF signals for iron and steel production GEM in Eastern China. All the results

301   above collectively confirmed that the PMF results were robust.

302   **3.2.2 Increasing contributions from natural surface emissions to ambient gaseous elemental**

303   **mercury**

304   Figure 6 summarizes the contributions of natural surface emissions and anthropogenic

305   emissions to GEM on seasonal basis from 2015 – 2018. The contributions of natural surface

306   emissions to GEM were ~40% higher in summer (1.15 ± 0.60 ng/m^3) than winter (0.82 ± 0.57 ng/m^3).

307   Besides, the contributions of natural surface emissions to GEM exhibited an upward trend, e.g.,

308   increased from 33% to 53% in spring, 47% to 62% in summer, 49% to 60% in autumn, and 34% to

309   52% in winter, from 2015-2018 (Figure 6). In contrast, the contributions from anthropogenic sources

310   to GEM showed a downward trend, of which the decreased contribution from coal combustion

311   accounted the most. Coal combustion has been widely regarded as the dominant anthropogenic

312   source of mercury emissions at the global scale, and China is known as the largest coal producer

313   and consumer in the world (Zhang et al., 2012;Wu et al., 2006). Since 2013, a series of key air

314   pollution control measures have been applied in China to reduce the emission of air pollutants

315   (Zheng et al., 2018). YRD regions also took actions by regulating on the amount of coal

316   consumption, promoting renewable energy development and so on (Zheng et al., 2016). Hence, the

317   decreased contribution of coal combustion was attributed to the implementation of aggressive air

318   pollutant control measures in China in recent years, which subsequently led to an increase in the

319   relative contribution of natural surface emissions to GEM.

320   The absolute GEM concentrations contributed by both natural surface emissions and

321   anthropogenic emissions can be extracted from the PMF modeling results. Figure 7 exhibits the

322   monthly and yearly profiles from 2015 to 2018. Strong seasonal cycles of GEM contributed by

323   natural surface emissions were seen, corresponding to the seasonal pattern of ambient temperature

324   (Figure 7g) and the simulated monthly Hg fluxes from natural surface emissions in China (Wang et

325   al., 2016). The annual GEM concentration contributed by natural surface emissions was estimated

326   to be 1.04 ± 0.55 ng/m^3, 1.10 ± 0.56 ng/m^3, 1.13 ± 0.56 ng/m^3, and 1.00 ± 0.45 ng/m^3 from 2015 to

327   2018, respectively (Figure 7a & 7b), which almost remained unchanged. This could be mainly

328   explained by the little variation of annual temperature (Fig. 7h) and wind pattern from 2015 to 2018

329   (Fig. S33). On the contrary, the annual GEM concentration contributed by anthropogenic emissions

330   was estimated to be 1.53 ± 1.04 ng/m^3, 1.26 ± 0.78 ng/m^3, 1.23 ± 0.95 ng/m^3, and 0.82 ± 0.58 ng/m^3

331   from 2015 to 2018, respectively, showing an obvious decreasing trend (Figure 7c & 7d). It was

332   noted that the GEM concentration contributed by anthropogenic emissions dropped the most from

333   2017 to 2018 with a rate of around 40%. By referring to the Table S3, SO_2 and CO also decreased

334   significantly of about 35% and 18%. As SO_2 and CO were the main primary gaseous pollutants

335   emitted from fuel combustions, their sharp decreases indicated the significant reduction of

336   anthropogenic emissions which was probably responsible for large drop of GEM from 2017 to 2018.

337   Overall, the relative contribution of natural surface emissions to ambient GEM was on the rise, e.g.,

338   from 41% in 2015 to 57% in 2018 on annual average (Figures 7e & 7f).

339

340   **4. Conclusions and Implications**

341   Through a four-year continuous measurement of GEM in the suburbs of Shanghai, a clear

342   decreasing trend was observed with the rate of -0.32±0.07 ng m^{-3} yr^{-1}, which was mainly due to the

343   reduction of anthropogenic mercury emissions. The lower decreasing rate in warm seasons than in

344   cold seasons and the high correlation between GEM concentrations and temperature suggested that

345   natural surface emissions significantly impacted the GEM concentrations. By demonstrating that

346   temperature and NH_3 can well serve as tracers of natural surface mercury emissions, distinguishing

347   natural vs. anthropogenic contributions to GEM was doable by introducing these tracers into the

348   PMF model. The results indicated that the contribution from anthropogenic mercury emissions was

349   declining, especially from coal combustion. The annual absolute contributions of natural surface

350   emissions were in the range of 1.00-1.13 ng/m^3, and the relative contribution of natural surface

351   emissions to GEM increasing form 41% in 2015 to 57% in 2018.

352   Measurements of GEM and other pollutants in a regional background area in Eastern China

353   demonstrated the effectiveness of emission control policies in this and surrounding regions in China

354   in recent years. The decreasing contributions from anthropogenic sources and the relatively stable

355   contributions from natural surface emissions to the ambient GEM have resulted in the relative

356   contributions of natural surface emissions surpassing those of anthropogenic emissions in more

357   recent years. This trend will likely continue for some years considering the current pollution levels

358   in China which needs further pollution abatement. This implies that even though the anthropogenic

359   emissions of mercury would continue to decrease, the legacy mercury in the natural surfaces will

360   continue to emit steadily for a long period of time. In addition, the natural release of mercury could

361   be enhanced under climate warming scenario. Hence, the atmospheric mercury concentration in

362   YRD or other parts of China will remain at relatively high levels in the near future, which brings

363   big challenges to China's policies on mercury emissions reduction. The methodology developed in

364   the present study could also shed some light on source apportionment of atmospheric mercury in

365   the other regions of the world, and has potential for improving emission databases from natural

366   surfaces where ambient GEM and auxiliary data are available.

It has to be noted that according to our results, ship emission was identified to be an important source of mercury which hasn't been included in previous emission inventory studies. Mercury emission factors from shipping are lacking and field measurements will be needed to verify it. Moreover, we realize that the application of PMF in the source apportionment of atmospheric mercury sources has certain limitations. Source-specific indicators are preferred, however, most indicators used for source identification have multiple sources, which have added uncertainties to our results. We suggest that in future research, the application of the PMF model is limited to the separation of the natural and total anthropogenic sources of GEM, which has been proved to be credible.

Acknowledgments

The authors acknowledge support of the National Key R&D Program of China (2018YFC0213105), the National Natural Science Foundation of China (91644105, 21777029), and the Natural Science Foundation of Shanghai (18230722600,19ZR1421100).

Author contribution

X.Q. and K. H. designed this study. X.Q. performed measurements and data analysis. X.W., Q.F., Q.Z., Y.L., and J.H. performed data collection. X.Q., L.Z., K.H., and C.D. wrote the paper. All have commented and reviewed the paper.

Competing interests

The authors declare that they have no conflict of interest.

Data availability

All data used in this study can be requested from K.H. (huangkan@fudan.edu.cn).

References:

Carslaw, D., Beevers, S., Ropkins, K., and Bell, M.: Detecting and quantifying aircraft and other on-airport contributions to ambient nitrogen oxides in the vicinity of a large international airport, Atmospheric Environment, 40, 5424-5434, 10.1016/j.atmosenv.2006.04.062, 2006.

Carslaw, D. C., and Ropkins, K.: openair — An R package for air quality data analysis, Environmental Modelling & Software, 27-28, 52-61, 10.1016/j.envsoft.2011.09.008, 2012.

399 Chang, Y., Zou, Z., Deng, C., Huang, K., Collett, J. L., Lin, J., and Zhuang, G.: The importance of vehicle
400 emissions as a source of atmospheric ammonia in the megacity of Shanghai, Atmospheric Chemistry and
401 Physics, 16, 3577-3594, 10.5194/acp-16-3577-2016, 2016.

402 Chang, Y., Deng, C., Cao, F., Cao, C., Zou, Z., Liu, S., Lee, X., Li, J., Zhang, G., and Zhang, Y.:
403 Assessment of carbonaceous aerosols in Shanghai, China - Part 1: long-term evolution, seasonal
404 variations, and meteorological effects, Atmospheric Chemistry and Physics, 17, 9945-9964, 10.5194/acp-
405 17-9945-2017, 2017.

406 Cheng, I., Xu, X., and Zhang, L.: Overview of receptor-based source apportionment studies for speciated
407 atmospheric mercury, Atmos. Chem. Phys., 15, 7877-7895, 10.5194/acp-15-7877-2015, 2015.

408 Clarkson, T. W., and Magos, L.: The toxicology of mercury and its chemical compounds, Crit. Rev.
409 Toxicol., 36, 609-662, 10.1080/10408440600845619, 2006.

410 Driscoll, C. T., Mason, R. P., Chan, H. M., Jacob, D. J., and Pirrone, N.: Mercury as a global pollutant:
411 sources, pathways, and effects, Environmental science & technology, 47, 4967-4983, 10.1021/es305071v,
412 2013a.

413 Driscoll, C. T., Mason, R. P., Chan, H. M., Jacob, D. J., and Pirrone, N.: Mercury as a Global Pollutant:
414 Sources, Pathways, and Effects, Environmental science & technology, 47, 4967-4983, 2013b.

415 Duan, L., Wang, X., Wang, D., Duan, Y., Cheng, N., and Xiu, G.: Atmospheric mercury speciation in
416 Shanghai, China, Sci. Total Environ., 578, 460-468, https://doi.org/10.1016/j.scitotenv.2016.10.209,
417 2017.

418 Feng, X. B., Wang, S. F., Qiu, G. A., Hou, Y. M., and Tang, S. L.: Total gaseous mercury emissions from
419 soil in Guiyang, Guizhou, China, J. Geophys. Res.-Atmos., 110, 2005.

420 Friedli, H. R., Arellano, A. F., Cinnirella, S., and Pirrone, N.: Initial Estimates of Mercury Emissions to
421 the Atmosphere from Global Biomass Burning, Environmental science & technology, 43, 3507-3513,
422 10.1021/es802703g, 2009.

423 Fu, X. W., Feng, X. B., Sommar, J., and Wang, S. F.: A review of studies on atmospheric mercury in
424 China, Sci. Total Environ., 421, 73-81, 10.1016/j.scitotenv.2011.09.089, 2012.

425 Gibson, M. D., Haelssig, J., Pierce, J. R., Parrington, M., Franklin, J. E., Hopper, J. T., Li, Z., and Ward,
426 T. J.: A comparison of four receptor models used to quantify the boreal wildfire smoke contribution to
427 surface PM2.5 in Halifax, Nova Scotia during the BORTAS-B experiment, Atmospheric Chemistry and
428 Physics, 15, 815-827, 10.5194/acp-15-815-2015, 2015.

429 Gustin, M. S., Lindberg, S. E., and Weisberg, P. J.: An update on the natural sources and sinks of
430 atmospheric mercury, Appl. Geochem., 23, 482-493, 10.1016/j.apgeochem.2007.12.010, 2008.

431 Horowitz, H. M., Jacob, D. J., Zhang, Y., Dibble, T. S., Slemr, F., Amos, H. M., Schmidt, J. A., Corbitt,
432 E. S., Marais, E. A., and Sunderland, E. M.: A new mechanism for atmospheric mercury redox chemistry:
433 implications for the global mercury budget, Atmospheric Chemistry and Physics, 17, 6353-6371,
434 10.5194/acp-17-6353-2017, 2017.

435 Howard, D., and Edwards, G. C.: Mercury fluxes over an Australian alpine grassland and observation of
436 nocturnal atmospheric mercury depletion events, Atmospheric Chemistry and Physics, 18, 129-142, 2018.

437 Kerr, G. H., and Waugh, D. W.: Connections between summer air pollution and stagnation,
438 Environmental Research Letters, 13, 10.1088/1748-9326/aad2e2, 2018.

439 Kerr, G. H., Waugh, D. W., Strode, S. A., Steenrod, S. D., Oman, L. D., and Strahan, S. E.: Disentangling
440 the Drivers of the Summertime Ozone-Temperature Relationship Over the United States, 124, 10503-
441 10524, 10.1029/2019jd030572, 2019.

442 Kocman, D., Horvat, M., Pirrone, N., and Cinnirella, S.: Contribution of contaminated sites to the global

443   mercury budget, Environmental Research, 125, 160-170, 10.1016/j.envres.2012.12.011, 2013.

444   Landis, M. S., and Keeler, G. J.: Atmospheric mercury deposition to Lake Michigan during the Lake

445   Michigan Mass Balance Study, Environmental science & technology, 36, 4518-4524, 10.1021/es011217b,

446   2002.

447   Lindberg, S. E., Zhang, H., Vette, A. F., Gustin, M. S., Barnett, M. O., and Kuiken, T.: Dynamic flux

448   chamber measurement of gaseous mercury emission fluxes over soils: Part 2 - effect of flushing flow rate

449   and verification of a two-resistance exchange interface simulation model, Atmospheric Environment, 36,

450   847-859, 10.1016/s1352-2310(01)00502-7, 2002.

451   Liu, K., Wu, Q., Wang, L., Wang, S., Liu, T., Ding, D., Tang, Y., Li, G., Tian, H., Duan, L., Wang, X., Fu,

452   X., Feng, X., and Hao, J.: Measure-Specific Effectiveness of Air Pollution Control on China's

453   Atmospheric Mercury Concentration and Deposition during 2013-2017, Environmental science &

454   technology, 10.1021/acs.est.9b02428, 2019a.

455   Liu, K., Wu, Q., Wang, L., Wang, S., Liu, T., Ding, D., Tang, Y., Li, G., Tian, H., Duan, L., Wang, X., Fu,

456   X., Feng, X., and Hao, J.: Measure-Specific Effectiveness of Air Pollution Control on China's

457   Atmospheric Mercury Concentration and Deposition during 2013-2017, Environmental science &

458   technology, 53, 8938-8946, 10.1021/acs.est.9b02428, 2019b.

459   Mao, H., Talbot, R. W., Sigler, J. M., Sive, B. C., and Hegarty, J. D.: Seasonal and diurnal variations of

460   Hg degrees over New England, Atmospheric Chemistry and Physics, 8, 1403-1421, 10.5194/acp-8-1403-

461   2008, 2008.

462   Mason, R. P., and Sheu, G. R.: Role of the ocean in the global mercury cycle, Global Biogeochemical

463   Cycles, 16, 40-41-40-14, 10.1029/2001gb001440, 2002.

464   Mason, R. P.: Mercury Emissions from Natural Processes and their Importance in the Global Mercury

465   Cycle, Mercury Fate and Transport in the Global Atmosphere: Emissions, Measurements and Models,

466   edited by: Pirrone, N., and Mason, R., 173-191 pp., 2009.

467   Moore, C., and Carpi, A.: Mechanisms of the emission of mercury from soil: Role of UV radiation, J.

468   Geophys. Res.-Atmos., 110, 10.1029/2004jd005567, 2005.

469   Pannu, R., Siciliano, S. D., and O'Driscoll, N. J.: Quantifying the effects of soil temperature, moisture

470   and sterilization on elemental mercury formation in boreal soils, Environmental Pollution, 193, 138-146,

471   10.1016/j.envpol.2014.06.023, 2014.

472   Pirrone, N., Cinnirella, S., Feng, X., Finkelman, R. B., Friedli, H. R., Leaner, J., Mason, R., Mukherjee,

473   A. B., Stracher, G. B., Streets, D. G., and Telmer, K.: Global mercury emissions to the atmosphere from

474   anthropogenic and natural sources, Atmos. Chem. Phys., 10, 5951-5964, 10.5194/acp-10-5951-2010,

475   2010.

476   Poissant, L., and Casimir, A.: Water-air and soil-air exchange rate of total gaseous mercury measured at

477   background sites, Atmospheric Environment, 32, 883-893, 10.1016/s1352-2310(97)00132-5, 1998.

478   Polissar, A. V., Hopke, P. K., and Paatero, P.: Atmospheric aerosol over Alaska - 2. Elemental composition

479   and sources, J. Geophys. Res.-Atmos., 103, 19045-19057, 10.1029/98jd01212, 1998.

480   Qin, X., Wang, X., Shi, Y., Yu, G., Zhao, N., Lin, Y., Fu, Q., Wang, D., Xie, Z., Deng, C., and Huang, K.:

481   Characteristics of atmospheric mercury in a suburban area of east China: sources, formation mechanisms,

482   and regional transport, Atmos. Chem. Phys., 19, 5923-5940, 10.5194/acp-19-5923-2019, 2019.

483   Quinones, J. L., and Anthony, C. J. J. o. E. Q.: An Investigation of the Kinetic Processes Influencing

484   Mercury Emissions from Sand and Soil Samples of Varying Thickness, 40, 647-, 2011.

485   Schnell, J. L., and Prather, M. J.: Co-occurrence of extremes in surface ozone, particulate matter, and

486   temperature over eastern North America, 114, 2854-2859, 10.1073/pnas.1614453114 %J Proceedings of

487   the National Academy of Sciences, 2017.

488   Schroeder, W. H., and Munthe, J.: Atmospheric mercury - An overview, Atmospheric Environment, 32,
489   809-822, 10.1016/s1352-2310(97)00293-8, 1998.

490   Sommar, J., Zhu, W., Shang, L., Lin, C.-J., and Feng, X.: Seasonal variations in metallic mercury (Hg-0)
491   vapor exchange over biannual wheat-corn rotation cropland in the North China Plain, Biogeosciences,
492   13, 2029-2049, 10.5194/bg-13-2029-2016, 2016.

493   Song, S., Selin, N. E., Soerensen, A. L., Angot, H., Artz, R., Brooks, S., Brunke, E. G., Conley, G.,
494   Dommergue, A., Ebinghaus, R., Holsen, T. M., Jaffe, D. A., Kang, S., Kelley, P., Luke, W. T., Magand,
495   O., Marumoto, K., Pfaffhuber, K. A., Ren, X., Sheu, G. R., Slemr, F., Warneke, T., Weigelt, A., Weiss-
496   Penzias, P., Wip, D. C., and Zhang, Q.: Top-down constraints on atmospheric mercury emissions and
497   implications for global biogeochemical cycling, Atmospheric Chemistry and Physics, 15, 7103-7125,
498   10.5194/acp-15-7103-2015, 2015.

499   Streets, D. G., Devane, M. K., Lu, Z. F., Bond, T. C., Sunderland, E. M., and Jacob, D. J.: All-Time
500   Releases of Mercury to the Atmosphere from Human Activities, Environmental science & technology,
501   45, 10485-10491, 10.1021/es202765m, 2011.

502   Tang, Y., Wang, S. X., Wu, Q. R., Liu, K. Y., Wang, L., Li, S., Gao, W., Zhang, L., Zheng, H. T., Li, Z.
503   J., and Hao, J. M.: Recent decrease trend of atmospheric mercury concentrations in East China: the
504   influence of anthropogenic emissions, Atmospheric Chemistry and Physics, 18, 8279-8291, 10.5194/acp-
505   18-8279-2018, 2018.

506   Wang, D. Y., He, L., Shi, X. J., Wei, S. Q., and Feng, X. B.: Release flux of mercury from different
507   environmental surfaces in Chongqing, China, Chemosphere, 64, 1845-1854,
508   10.1016/j.chemosphere.2006.01.054, 2006.

509   Wang, L., Wang, S. X., Zhang, L., Wang, Y. X., Zhang, Y. X., Nielsen, C., McElroy, M. B., and Hao, J.
510   M.: Source apportionment of atmospheric mercury pollution in China using the GEOS-Chem model,
511   Environmental Pollution, 190, 166-175, 10.1016/j.envpol.2014.03.011, 2014a.

512   Wang, X., Lin, C. J., and Feng, X.: Sensitivity analysis of an updated bidirectional air-surface exchange
513   model for elemental mercury vapor, Atmospheric Chemistry and Physics, 14, 6273-6287, 10.5194/acp-
514   14-6273-2014, 2014b.

515   Wang, X., Lin, C.-J., Yuan, W., Sommar, J., Zhu, W., and Feng, X.: Emission-dominated gas exchange
516   of elemental mercury vapor over natural
517   surfaces in China, Atmospheric Chemistry and Physics, 16, 11125-11143, 10.5194/acp-16-11125-2016,
518   2016.

519   Wright, L. P., and Zhang, L. M.: An approach estimating bidirectional air-surface exchange for gaseous
520   elemental mercury at AMNet sites, Journal of Advances in Modeling Earth Systems, 7, 35-49,
521   10.1002/2014ms000367, 2015.

522   Wright, L. P., Zhang, L., Cheng, I., Aherne, J., and Wentworth, G. R.: Impacts and Effects Indicators of
523   Atmospheric Deposition of Major Pollutants to Various Ecosystems - A Review, Aerosol Air Qual. Res.,
524   18, 1953-1992, 10.4209/aaqr.2018.03.0107, 2018.

525   Wu, Q. R., Wang, S. X., Li, G. L., Liang, S., Lin, C. J., Wang, Y. F., Cai, S. Y., Liu, K. Y., and Hao, J. M.:
526   Temporal Trend and Spatial Distribution of Speciated Atmospheric Mercury Emissions in China During
527   1978-2014, Environmental science & technology, 50, 13428-13435, 10.1021/acs.est.6b04308, 2016.

528   Wu, Y., Wang, S. X., Streets, D. G., Hao, J. M., Chan, M., and Jiang, J. K.: Trends in anthropogenic
529   mercury emissions in China from 1995 to 2003, Environmental science & technology, 40, 5312-5318,
530   10.1021/es060406x, 2006.

531 Xu, X., Liao, Y., Cheng, I., and Zhang, L.: Potential sources and processes affecting speciated
532 atmospheric mercury at Kejimkujik National Park, Canada: comparison of receptor models and data
533 treatment methods, Atmospheric Chemistry and Physics, 17, 1381-1400, 10.5194/acp-17-1381-2017,
534 2017.
535 Xu, X. H., Yang, X. S., Miller, D. R., Helble, J. J., and Carley, R. J.: Formulation of bi-directional
536 atmosphere-surface exchanges of elemental mercury, Atmospheric Environment, 33, 4345-4355,
537 10.1016/s1352-2310(99)00245-9, 1999.
538 Yu, Y., He, S., Wu, X., Zhang, C., Yao, Y., Liao, H., Wang, Q., and Xie, M.: PM2.5 elements at an urban
539 site in Yangtze River Delta, China: High time-resolved measurement and the application in source
540 apportionment, Environ Pollut, 253, 1089-1099, 10.1016/j.envpol.2019.07.096, 2019.
541 Zhang, L., Wright, L. P., and Asman, W. A. H.: Bi-directional air-surface exchange of atmospheric
542 ammonia: A review of measurements and a development of a big-leaf model for applications in regional-
543 scale air-quality models, J. Geophys. Res.-Atmos., 115, 10.1029/2009jd013589, 2010.
544 Zhang, L., Wang, S. X., Meng, Y., and Hao, J. M.: Influence of Mercury and Chlorine Content of Coal
545 on Mercury Emissions from Coal-Fired Power Plants in China, Environmental science & technology, 46,
546 6385-6392, 10.1021/es300286n, 2012.
547 Zhang, L., Wang, S., Wang, L., Wu, Y., Duan, L., Wu, Q., Wang, F., Yang, M., Yang, H., Hao, J., and Liu,
548 X.: Updated emission inventories for speciated atmospheric mercury from anthropogenic sources in
549 China, Environmental science & technology, 49, 3185-3194, 10.1021/es504840m, 2015.
550 Zhang, Y., Jacob, D. J., Horowitz, H. M., Chen, L., Amos, H. M., Krabbenhoft, D. P., Slemr, F., St Louis,
551 V. L., and Sunderland, E. M.: Observed decrease in atmospheric mercury explained by global decline in
552 anthropogenic emissions, Proc Natl Acad Sci U S A, 113, 526-531, 10.1073/pnas.1516312113, 2016.
553 Zheng, B., Tong, D., Li, M., Liu, F., Hong, C., Geng, G., Li, H., Li, X., Peng, L., Qi, J., Yan, L., Zhang,
554 Y., Zhao, H., Zheng, Y., He, K., and Zhang, Q.: Trends in China's anthropogenic emissions since 2010 as
555 the consequence of clean air actions, Atmospheric Chemistry and Physics, 18, 14095-14111,
556 10.5194/acp-18-14095-2018, 2018.
557 Zheng, J., Jiang, P., Qiao, W., Zhu, Y., and Kennedy, E.: Analysis of air pollution reduction and climate
558 change mitigation in the industry sector of Yangtze River Delta in China, Journal of Cleaner Production,
559 114, 314-322, 10.1016/j.jclepro.2015.07.011, 2016.
560 Zhu, W., Sommar, J., Lin, C. J., and Feng, X.: Mercury vapor air-surface exchange measured by
561 collocated micrometeorological and enclosure methods - Part II: Bias and uncertainty analysis,
562 Atmospheric Chemistry and Physics, 15, 5359-5376, 10.5194/acp-15-5359-2015, 2015.
563 Zhu, W., Lin, C.-J., Wang, X., Sommar, J., Fu, X., and Feng, X.: Global observations and modeling of
564 atmosphere–surface exchange of elemental mercury: a critical review, Atmospheric Chemistry and
565 Physics, 16, 4451-4480, 10.5194/acp-16-4451-2016, 2016.

566
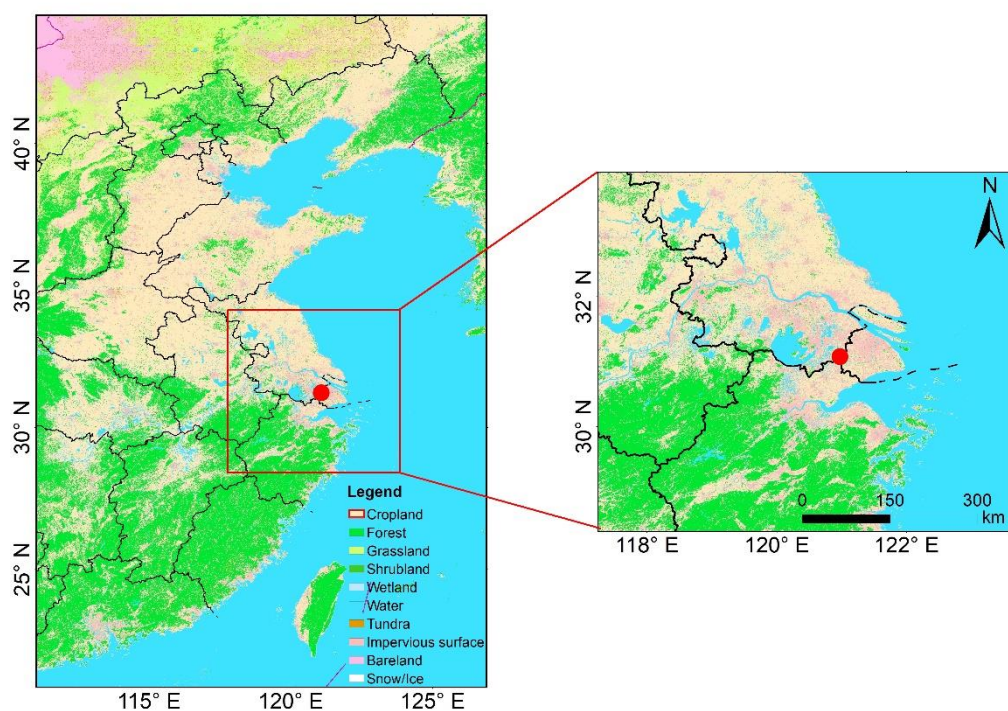
567   Figure 1. The location of the Dianshan Lake (DSL) site in Shanghai, China. Different colors in the

568   map represent different land cover types.

569
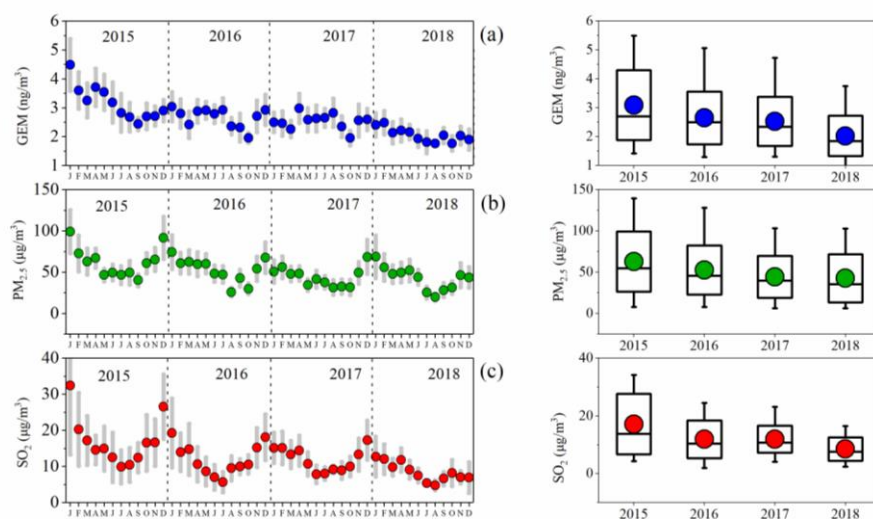
570

571   Figure 2. Monthly and annual variations of (a) GEM, (b) PM$_{2.5}$, and (c) SO$_2$ concentrations from

572   2015 to 2018.

573

574
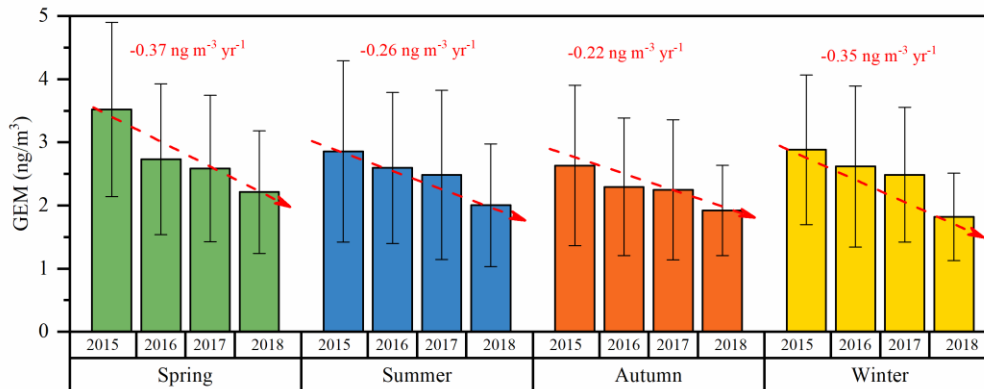
Figure 3. Seasonal variations of GEM concentrations from 2015 to 2018. The variation rates of GEM for each season are also shown in the figure.

577

578
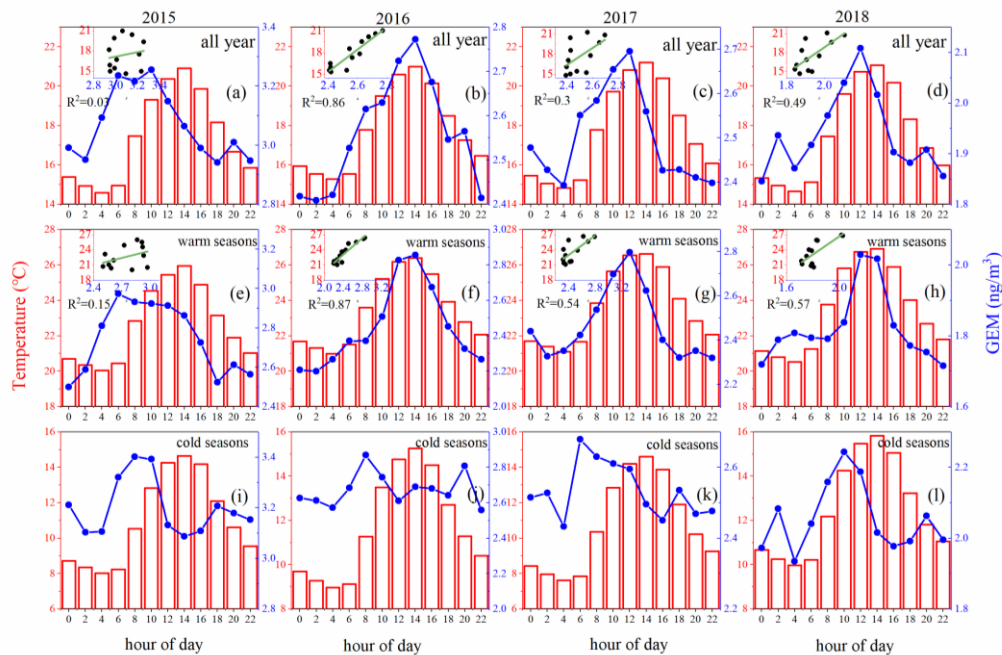
Figure 4. Diurnal patterns of bi-hourly GEM concentrations and temperature for the whole year (a-d), warm seasons (e-h), and cold seasons (i-l) during 2015 – 2018, respectively. The linear correlations between GEM and temperature are inserted as inner figures.

582

583

584
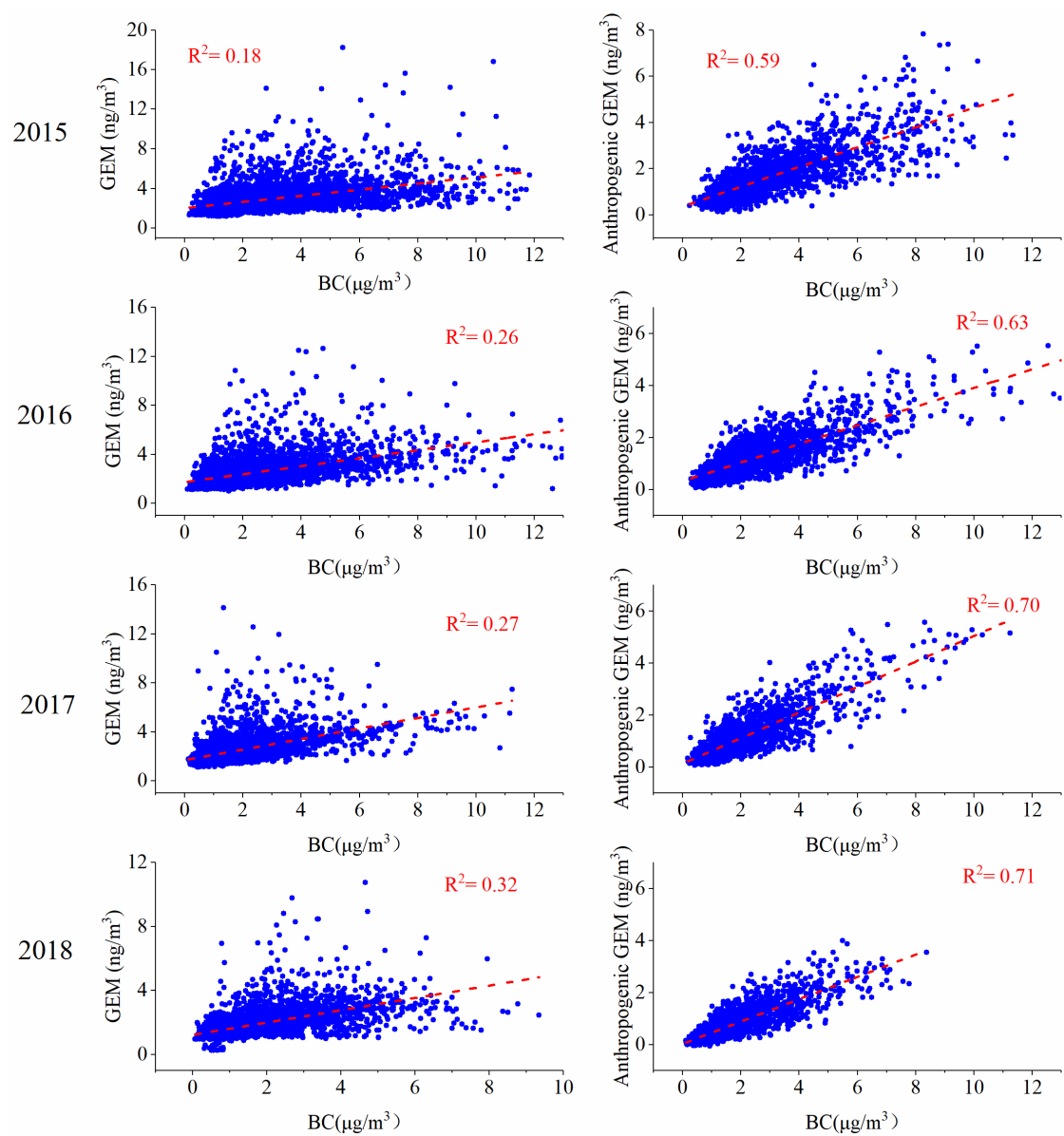
585

586 Figure 5. The relationship between observed GEM and BC, anthropogenic GEM (extracted from

587 PMF results) and BC during 2015 – 2018

588
589
590
591

592
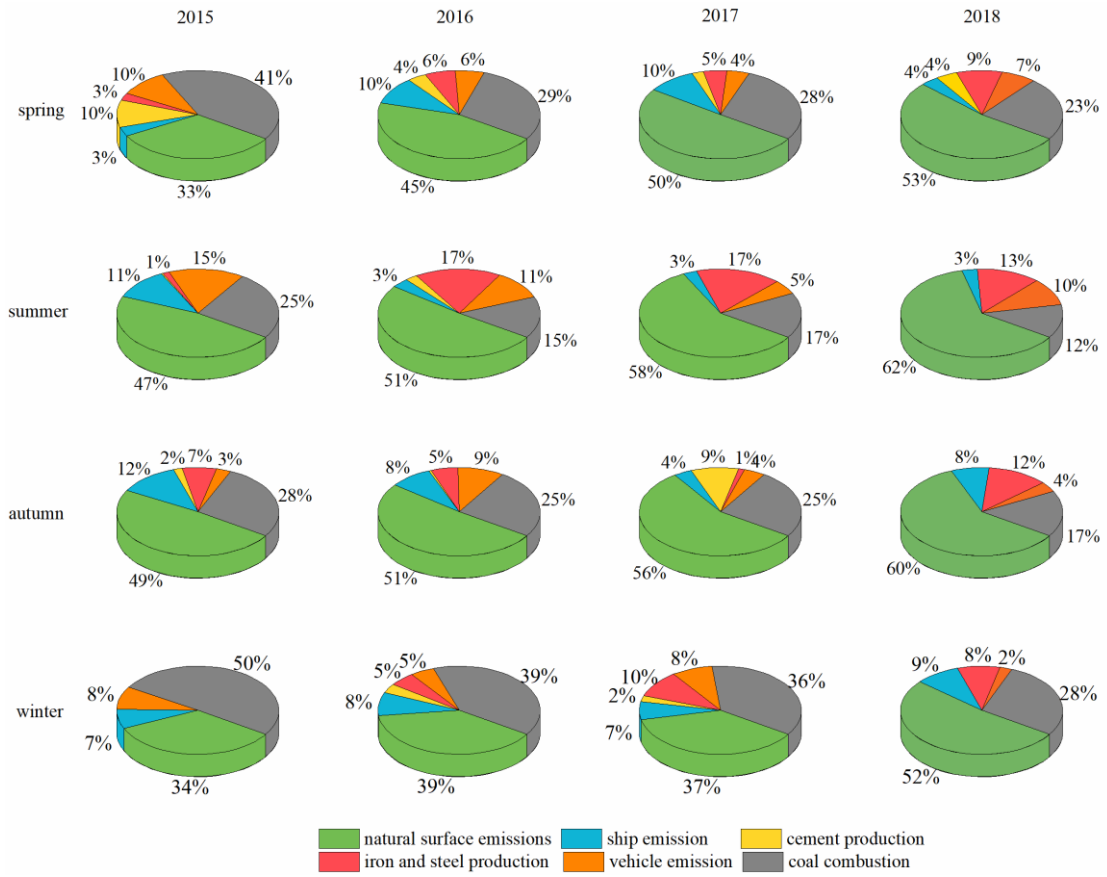
Figure 6. Contributions of natural surface emissions and anthropogenic sources to atmospheric

GEM in the four seasons during 2015 – 2018.

595

596
597
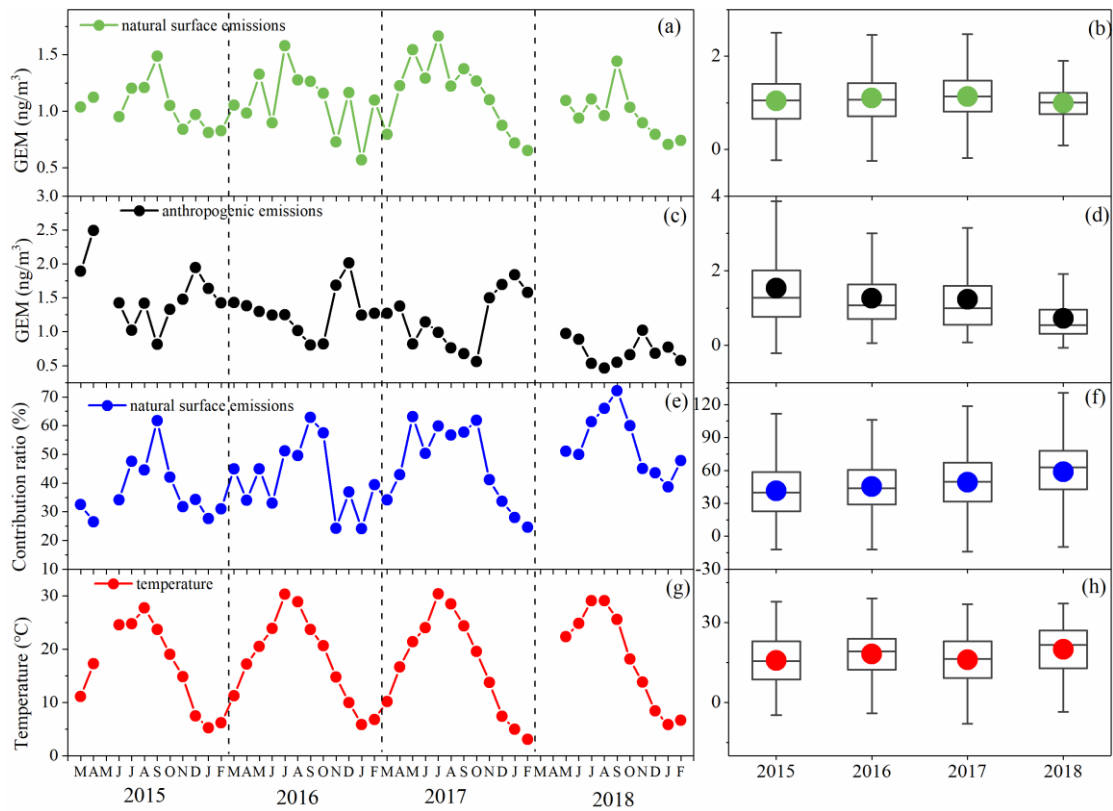
598

599 Figure 7. The monthly and annual GEM concentrations contributed by natural surface emissions (a-

600 b) and anthropogenic emissions (c-d) from 2015 to 2018. (e-f) The monthly and annual contribution

601 of natural surface emissions to GEM concentrations from 2015 to 2018. (g-h) The corresponding

602 ambient temperature from 2015 to 2018.